MHD CASSON NANOFLUID FLOW OVER A STRETCHING SURFACE EMBEDDED IN A POROUS MEDIUM: EFFECTS OF THERMAL RADIATION AND SLIP CONDITIONS

Article *in* Latin American applied research Pesquisa aplicada latino americana = Investigación aplicada latinoamericana · September 2021

DOI: 10.52292/j.laar.2021.523

CITATIONS
0

READS
207

6 authors, including:

Sameh E. Ahmed
South Valley University
186 PUBLICATIONS **2,779** CITATIONS
SEE PROFILE

R. A. Mohamed
South Valley University
59 PUBLICATIONS **1,015** CITATIONS
SEE PROFILE

Ali J. Chamkha
Kuwait College of Science and Technology
994 PUBLICATIONS **30,690** CITATIONS
SEE PROFILE

Mahmoud S. Soliman
South Valley University
14 PUBLICATIONS **45** CITATIONS
SEE PROFILE

MHD CASSON NANOFLUID FLOW OVER A STRETCHING SURFACE EMBEDDED IN A POROUS MEDIUM: EFFECTS OF THERMAL RADIATION AND SLIP CONDITIONS

R.A. MOHAMED†, S.E. AHMED‡, A.M. ALY‡, A.J. CHAMKHA§ and M.S. SOLIMAN†

† *Department of Mathematics, Faculty of Science, South valley university, Qena, Egypt.*
‡ *Department of Mathematics, Faculty of Science, Abha, King Khalid University, Saudi Arabia.*
§ *Faculty of Engineering, Kuwait College of Science and Technology, Doha District, 35004, Kuwait.*
E-mail: rabdalla_1953@yahoo.com, sehassan@kku.edu.sa, achamkha@pmu.edu.sa, ababdallah@kku.edu.sa, M.Soliman757@yahoo.com

***Abstract*— This article presents a numerical study for the magnetohydrodynamic flow of Casson nanofluid over a stretching sheet through a porous medium under effects each of non-linear thermal radiation, heat generation/absorption, Joule heating and slips boundary conditions. A two-phase nanofluid model is applied to represent the nanofluid mixture. The porous medium is represented via the Darcy model. A similar solution is obtained for the governing equations and a numerical treatment based on the Runge-Kutta method is conducted to the resulting system of equations. In this study, the controlling physical parameters are the Casson fluid parameter β, the magnetic field M, the non-linear thermal radiation parameter R, the Brownian motion parameter Nb and the thermophoresis parameter Nt. The obtained results revealed that an increase in the Casson parameter, magnetic field parameter and Darcy number reduces the skin friction coefficient while the increase in the non-linear thermal radiation and the heat generation and absorption lead to a decrease in the local Nusselt number.**

***Keywords*— Casson fluid, Magnetohydrodynam-ic, Nanofluid, Stretching sheet, thermal radiation.**

I. INTRODUCTION

One of the important non-Newtonian fluids is the Casson fluid. This type of fluid gains several attentions, since it can be transformed into a flexible solid material at small values of the shear stress. The Casson fluid follows the behavior of the Newtonian fluid when the stress attaching to the critical value and it has high viscosity when the shear rate is zero. The honey, human blood and tomato liquid have similar properties of the Casson fluid. In the literature, there are numerous studies on the impacts of the physical parameters in Casson fluid (Souayeh *et al*., 2019; Reddy, 2016; Tamoor *et al*., 2017; Hayat *et al*., 2011; Kataria and Patel, 2019a; Ullah *et al.,* 2017; Kumaran and Sandeep, 2017; Kamran *et al*., 2017; Nawaz e*t al.,* 2018). Souayeh *et al.* (2019) analyzed the Magnetohydrodynamic (MHD) Casson nanofluid along a thin needle under the effects of non-linear radiative heat transfer. Reddy (2016) considered the influences of thermal radiation and chemical reaction on MHD flow of a Casson fluid over exponentially stretching surface. Tamoor *et al.,* (2017) investigated the MHD flow of a Casson fluid over a stretching cylinder. The ramped wall temperature and ramped surface concentration were considered for Casson fluid over an exponentially accelerated plate by Kataria and Patel (2019a). Nawaz *et al.,* (2018) studied the MHD axisymmetric flow of a Casson fluid by considering variable thermal conductivity and free stream. In the recent years, MHD flows have been received numerous attentions due to their importance in several branches of the modern industries. Rehman *et al.* (2018) introduced a numerical analysis for the flow of MHD Casson nanofluid over a rotating disk. The Casson fluid with dissipative MHD under the variations on the chemical reaction and a heat source were considered by Ibrahim *et al.* (2017). Reddy *et al.* (2018a) adopted FEM method to study MHD natural convection in a Casson fluid. Hayat *et al.* (2013) introduced a series solution for three-dimensional flow of an Oldroyd-B fluid.

Adding nanometer-sized particles, (nanoparticles) in the base fluid forming a new fluid entitled nanofluid. The nanoparticles are made of metals, oxides, carbides, or carbon nanotubes. The common base fluids are water, ethylene glycol and oil. The nanofluid has several applications in heat transfer including engine cooling, microelectronics, fuel cells and heat exchanger. Pal *et al.* (2016) used a scaling group transformation to check the influences of the thermal radiation on MHD Casson nanofluid flow. Hayat *et al.* (2018) considered the Cattaneo-Christov double-diffusion theory of a three-dimensional flow of a viscoelastic nanofluid with impacts of the heat generation/absorption. Saqib *et al.* (2018) applied atangana–Baleanu fractional derivative to MHD channel flow of CMC-based-CNT's nanofluid through a porous medium. Kataria and Patel (2019b) studied MHD Casson fluid flow past oscillating porous plate with considering the ramped wall temperature. Also, Kataria and Mittal (2017) checked the influences of the magnetic field on the gravity-driven convection nanofluid flow past an oscillating plate. Chamkha and Aly (2010-2011) studied MHD free/mixed convection flow of a nanofluid past plate under different conditions. In addition, there are many problems related to the impacts of the magnetic field on a nanofluid over different plates (Ramzan *et al*., 2016; Kataria and Patel, 2018; Shit *et al*., 2017; Sulochana *et al.,* 2018; Prasad *et al*., 2018; Gaffar *et al*., 2015; Seth *et al.,* 2018; Kumar *et al*., 2020; Palaniammal and Saritha, 2018; Mehryan *et al*., 2019; Mehryan *et al*., 2018; Pop and Sheremet, 2016; Reddy *et al*., 2018b).

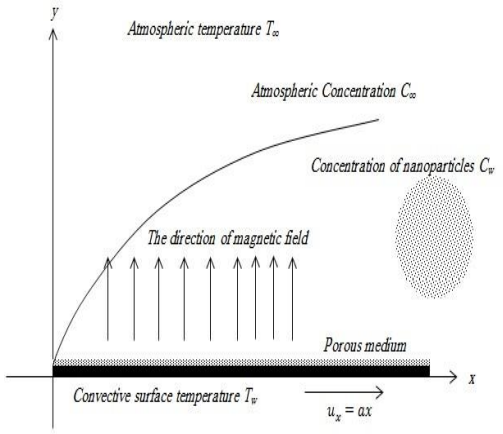

Fig. 1. A schematic diagram of the considered model.

For our knowledge, the authors ignored the case of MHD mixed convection flow of a non-Newtonian Casson nanofluid in the presence of non-linear thermal radiation, Joule heating and heat generation/absorption flow in a slip flow regime. Then, these works focus on the impacts of non-linear thermal radiation, Joule heating and heat generation/absorption for MHD mixed convection flow of a non-Newtonian Casson nanofluid. The presenting of the mathematical formulation and examination effects of the key parameters on the nanofluid flow and heat transfer characteristics were considered. The results revealed that the velocity profiles are decrease as magnetic field parameter, Darcy number; Casson fluid parameter β and the γ parameter are increase. In addition, the enhancement in nanoparticles volume fraction happens at higher values of several parameters such as magnetic field parameter, Darcy number, Casson fluid parameter β, γ parameter, thermo-phoresis parameter, Eckert number, Biot number and the heat source/sink parameter.

II. METHODS

A. Problem description

In Fig. 1, sketch of the current physical mode is presented. It consists of a stretching surface with velocity $U_w(x) = ax$. Constant temperature and concentration T_w and C_w are transmitted to the surface of the wall while the free stream temperature and the concentration are T_∞, C_∞. Uniform magnetic field is considered in the vertical direction and both of effects of a heat generation/absorption and thermal radiation are taken into account. Additionally, at the surface of the wall, slip condition and convective boundary conditions are assumed while the Joule heating term is including in the energy equation.

B. Mathematical formulation

The stress tensor in case of the Casson fluid is given by:

$$\tau_{ij} = \begin{cases} 2\left(\mu_p + \frac{p_y}{\sqrt{2\pi}}\right)e_{ij}, & \pi > \pi_c \\ 2\left(\mu_p + \frac{p_y}{\sqrt{2\pi}}\right)e_{ij}, & \pi < \pi_c \end{cases} \quad (1)$$

The (i,j) component of the deformation rate is e_{ij}, the product of e_{ij} with itself is $\pi_c = e_{ij}e_{ji}$ and the critical value of this product based on the non-Newtonian model is π_c. The basic equations governing for MHD flow of Casson nanofluid are given by;

$$\frac{\partial u}{\partial x} + \frac{\partial v}{\partial y} = 0, \quad (2)$$

$$u\frac{\partial u}{\partial x} + v\frac{\partial v}{\partial y} = \nu\left(1 + \frac{1}{\beta}\right)\frac{\partial^2 u}{\partial y^2} - \frac{\mu}{\rho K}u - \frac{\sigma B_0^2}{\rho}u, \quad (3)$$

$$u\frac{\partial T}{\partial x} + v\frac{\partial T}{\partial y} = \alpha\left(\frac{\partial^2 T}{\partial y^2}\right) + \frac{Q}{(\rho c_p)_f}(T - T_\infty) - \frac{1}{(\rho c_p)_f}\frac{\partial q_r}{\partial y} + \tau\left\{D_B\left(\frac{\partial C}{\partial y}\frac{\partial T}{\partial y}\right) + \left(\frac{D_T}{T_\infty}\right)\left[\left(\frac{\partial T}{\partial y}\right)^2\right]\right\} + \frac{\sigma B_0^2 u^2}{\rho c_p} \quad (4)$$

$$u\frac{\partial C}{\partial x} + v\frac{\partial C}{\partial y} = D_B\frac{\partial^2 C}{\partial y^2} + \left(\frac{D_T}{T_\infty}\right)\left(\frac{\partial^2 T}{\partial y^2}\right) \quad (5)$$

In the previous equations, u and v are the velocity components along the x and y axes, respectively. α is the diffusivity, ρ is density of the fluid, ρ_p is density of the nanoparticles, ν is the kinematic viscosity of the fluid, T is the fluid temperature, T_∞ is ambient fluid temperature, Q is the dimensional heat generation/absorption, D_B is the Brownian diffusion coefficient, D_T is the thermophoresis diffusion, c_p is the specific heat at constant pressure, $(\rho c_p)_f$ is the heat capacity of fluid, $q_r = -\frac{4\sigma^*}{3k^*}\frac{\partial T^4}{\partial y}$ is the nonlinear radiative heat flux where σ^* and k^* are the Stefan-Boltzmann constant and the mean absorption coefficient respectively, k is the thermal conductivity, C is the nanoparticles volume fraction and $\tau = (\rho c_p)_p/(\rho c_p)_f$ is the ratio of the effective heat capacity of nanoparticle material to the effective heat capacity of the base fluid. The subjected boundary conditions are assumed as:

$$\left.\begin{aligned} u = U_w(x) + \gamma_0\left(1 + \frac{1}{\beta}\right)\frac{\partial u}{\partial y}, \\ v = 0, -k\frac{\partial T}{\partial y} = h(T_w - T), \\ D_B\frac{\partial C}{\partial y} + \frac{D_T}{T_\infty}\frac{\partial T}{\partial y} = 0, \text{ at } y = 0 \end{aligned}\right\} \quad (6)$$

$$u \to 0, v \to 0, T \to T_\infty, C \to C_\infty, \text{ as } y \to \infty. \quad (7)$$

where γ_0, k and h represent the proportional constant of slip velocity, the thermal conductivity and the coefficient of convective heat transfer.

Now, the following similarity transformations are proposed:

$$\left.\begin{aligned} u = U_w f'(\eta), v = -\sqrt{\frac{\nu U_w}{x}}f(\eta), \\ \theta(\eta) = \frac{T - T_\infty}{T_w - T_\infty}, \ \phi(\eta) = \frac{C - C_\infty}{C_\infty}, \\ \eta = \sqrt{\frac{U_w}{\nu x}}\, y, \end{aligned}\right\} \quad (8)$$

where $f'(\eta)$, $\theta(\eta)$ and $\phi(\eta)$ represent the velocity, the temperature and the concentration of nanoparticles distributions, respectively. The similarity transformations (8) are used to convert the governing partial differential Eqs. (3–5) with the boundary conditions (6) and (7) into a system of ordinary differential equations as:

$$f'''(\eta) + \frac{\beta}{1+\beta}\left(f(\eta)f''(\eta) - f'^2(\eta) - (M + Da)f'(\eta)\right) = 0. \quad (9)$$

$$\theta''(\eta) + Pr\left(S\theta(\eta) + Nb\theta'(\eta)\phi'(\eta) + Nt\theta'^2(\eta) + R\left((Ct + \theta(\eta))^3\phi'(\eta)\right)' + EcMf'^2(\eta) + f(\eta)\theta'(\eta)\right) = 0 \quad (10)$$

$$\phi''(\eta) + Lef\phi'(\eta) + \frac{Nt}{Nb}\theta''(\eta) = 0, \quad (11)$$

with the boundary conditions:

$$\left.\begin{aligned} f(0)=0, f'(0)=1+\gamma\left(1+\frac{1}{\beta}\right)f''(0),\\ \theta'(0)=-Bi\big(1-\theta(0)\big),\\ Nb\phi'(0)+Nt\,\theta'(0)=0 \end{aligned}\right\} \quad (12)$$

$$f'(\infty)\to 0, \theta(\infty)\to 0, \phi(\infty)\to 0, \quad (13)$$

where β is the Casson fluid parameter and the following parameters are defined:

$Bi=\sqrt{v/a}\,h_f/k$: the Biot number.
$S=Q/a(\rho c_p)_f$: the heat source/sink parameter.
$Nb=\tau D_B C_\infty/v$: the Brownian motion parameter.
$Nt=\tau D_T(T_w-T_\infty)/(vT_\infty)$: the thermophoresis parameter.
$Le=v/D_B$: the Lewis number.
$Da=\mu/a\rho K$: the Darcy number.
$R=16\sigma^*(T_w-T_\infty)^3/(3kk^*)$: the non-linear thermal radiation parameter.
$Pr=v/\alpha$: the Prandtl number.
$M=\sigma B_0^2/(\rho a)$: the magnetic field parameter.
$\gamma=\gamma_0\sqrt{a/v}$: the nondimensional slip velocity parameter.
$Ec=U_w^2/(c_p(T_w-T_\infty))$: the Eckert number.
$Ct=T_\infty/(T_w-T_\infty)$: the ratio temperature parameter.

The skin friction coefficient and the local Nusselt number in case of the Casson nanofluid flow are expressed by:

$$C_f=\left(1+\frac{1}{\beta}\right)\frac{\tau_w}{\rho U_w^2}, \quad (14)$$

$$Nu_x=\frac{xq_w}{\alpha(T_w-T_\infty)}, \quad (15)$$

and the reader will note that the dimensionless mass flux represented by a Sherwood number Sh_x is now identically zero. q_w and τ_w is the heat flux and the shear stress along the stretching sheet respectively on the following mathematical formula:

$$q_w=-\alpha\left(\frac{\partial T}{\partial y}\right)_{y=0}+(q_r)_{y=0}, \quad (16)$$

$$\tau_w=\mu\left(\frac{\partial u}{\partial y}\right)_{y=0}, \quad (17)$$

the dimensionless form of Eqs. (14) and (15) can be written as:

$$Re_x^{1/2}C_f=\left(1+\frac{1}{\beta}\right)f''(0), \quad (18)$$

$$Re_x^{1/2}Nu_x=-\Big(1+R\big(Ct+\theta(0)\big)^3\Big)\theta'(0), \quad (19)$$

here, $Re_x=\frac{x}{v}U_w(x)$ is the local Reynolds number based on the stretching velocity $U_x(x)$.

C. Results and discussion

This part presents thorough discussions for all the obtained results. Influences of the controlling parameters, namely, the Casson fluid parameter β, the Biot number parameter Bi, the heat source/sink parameter S, the Brownian motion parameter Nb, the thermophoresis parameter Nt, the Lewis number Le, the Darcy number Da, the non-linear thermal radiation parameter R, the Prandtl number Pr, the magnetic field parameter M, the proportional constant of slip velocity γ, the Eckert number Ec, and the ratio temperature parameter Ct are examined using a set of the graphical results. Wide ranges of the gov erning parameters are taken into account to cover the physical insight, see results reported by Kamran *et al.* (2017), Kataria and Patel (2019b) and Kataria and Mittal (2017).

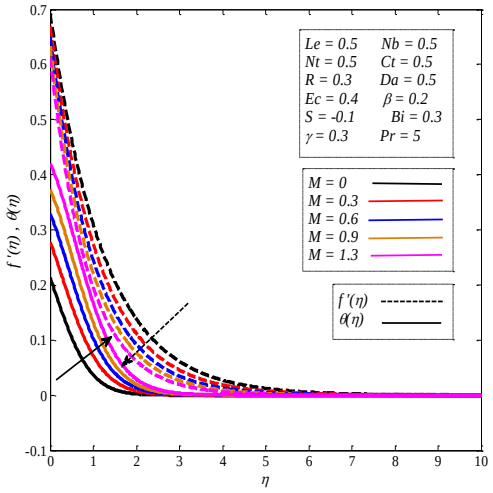

Fig. 2. Velocity and temperature profiles for variations of the magnetic field M.

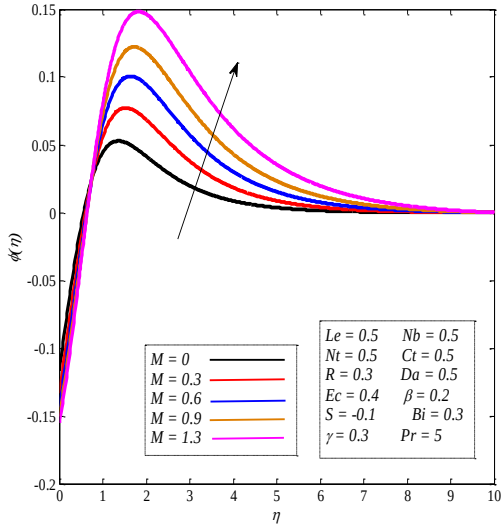

Fig. 3. Concentration of nanoparticles profile for variations of the magnetic field M.

Figures 2 and 3 show effects of the magnetic field parameter $0\le M\le 1.3$ on the distributions of the velocity, the temperature and the concentration of nanoparticles. It is noted that an increase in the magnetic force enhances both of the temperature and nanoparticles volume fraction while the Casson nanofluid velocity is reduced. Physically, presence of the magnetic force in the flow domain causes a generation of the Lorentz force; that works to resist the movement of the fluid.

To explain effects of values of the Casson fluid parameter $0\le\beta\le 1.3$ on velocity and distributions of the nanoparticles, it should be mentioned that the Casson fluid parameter β refers to the inverse relation between the yield stress and the rate of the fluid viscosity. So, an increase in the Casson fluid parameter β leads a shortage of decrease in the yield stress and increases the viscosity,

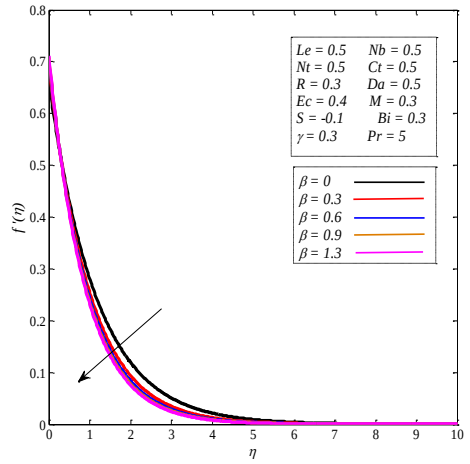

Fig. 4. temperature profile for variations of Casson nanofluid β.

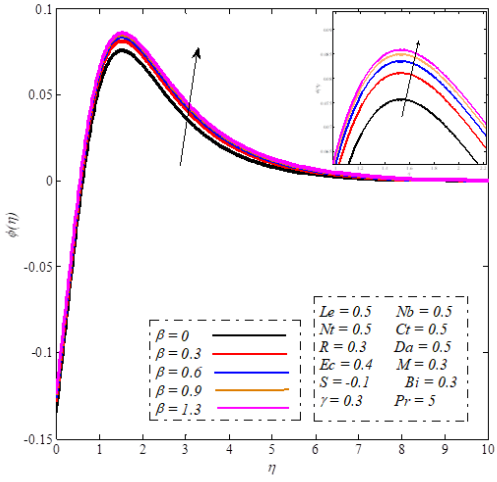

Fig. 5. Concentration of nanoparticles profile for variations of Casson fluid β.

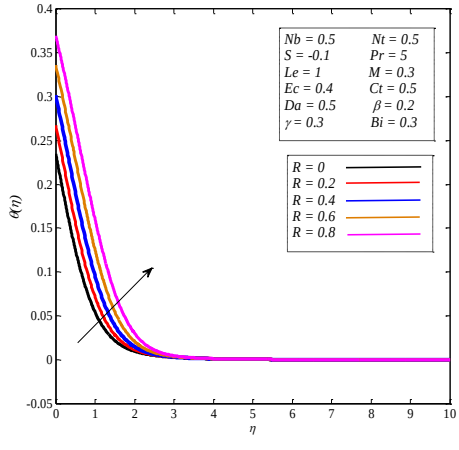

Fig. 6. Effect of the non-linear thermal radiation parameter R on the temperature profile.

leading to a decrease in the velocity of the fluid and increase in the rate of concentration of nanoparticles, as it can be seen in Figs. 4 and 5.

Figures 6, 7, 8 and 9 elucidate impacts of the non-linear thermal radiation parameter $0 \leq R \leq 0.8$ and ratio of

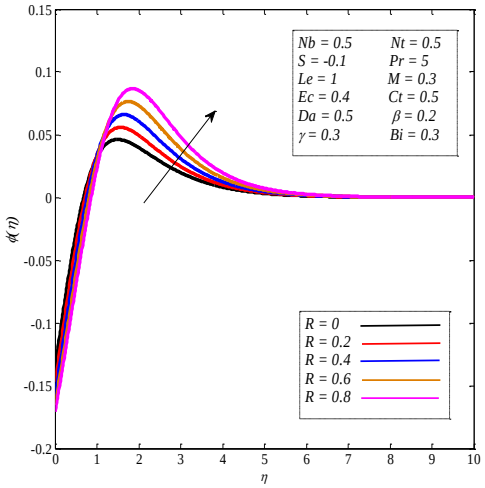

Fig. 7. Effect of the non-linear thermal radiation parameter R on the concentration of nanoparticles profile.

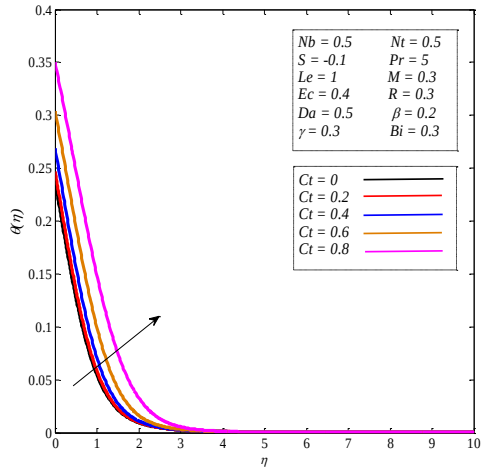

Fig. 8. Effect of the ratio temperature parameter Ct on the temperature profile.

the temperature parameter $0 \leq Ct \leq 0.8$ on profiles of the Casson nanofluid temperature $\theta(\eta)$ and the concentration of nanoparticles $\phi(\eta)$. It is clear that both of the temperature and the concentration of nanoparticles are supported by alteration of R and Ct. This behavior can be clarified by the fact that the increase in the non-linear thermal radiation parameter and ratio temperature parameter leads to generate an extra heat in the flow domain which in turn enhances both of the temperature and the concentration of nanoparticles.

Figures 10 and 11 explain influence of the Prandtl number $1 \leq Pr \leq 20$ on the distributions of the temperature and the concentration of nanoparticles. The results revealed that an increase in Pr reduces profiles of the temperature and concentration of the nanoparticles. The physical interpretation of this behavior is due to the weakness in the thermal conductivity of the Casson nanofluid resulting from the increase in Pr which reduces the temperature. On the other hand, an increase in the Prandtl number results in a decrease in the concentration of the nanoparticles within the fluid because of the strong inertia that leads

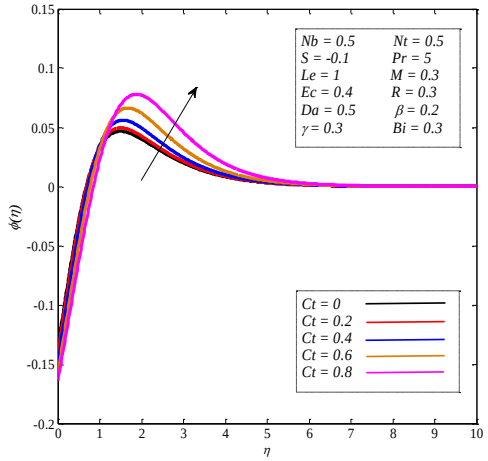

Fig. 9. Effect of the ratio temperature parameter Ct on the concentration of nanoparticles profile.

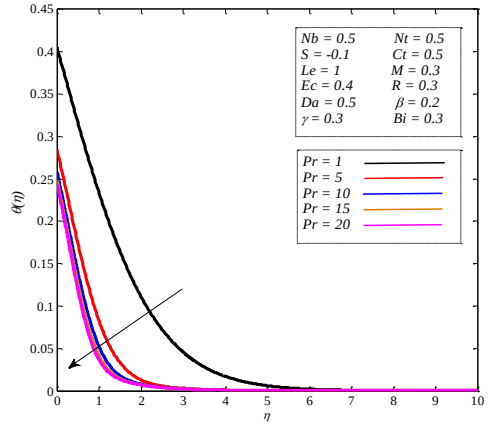

Fig. 10. Effect of the Prandtl number Pr on the temperature profile.

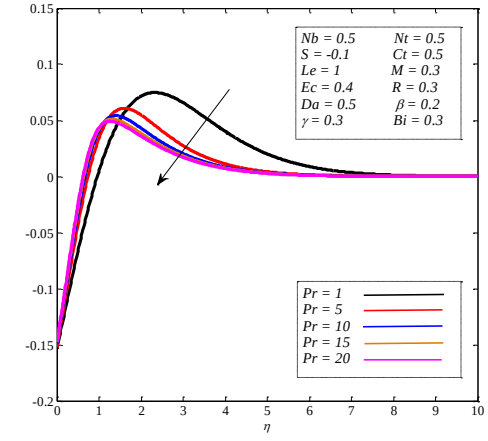

Fig. 11. Effect of the Prandtl number Pr on the concentration of nanoparticles profile.

to the removal of these particles from the surface of the fluid.

Figure 12 depicts the negative effectiveness of the Lewis number $1 \leq Le \leq 5$ on the concentration of nanoparticles distribution. In fact, strengthening the values of Lewis number Le means an enhancement of the thermal

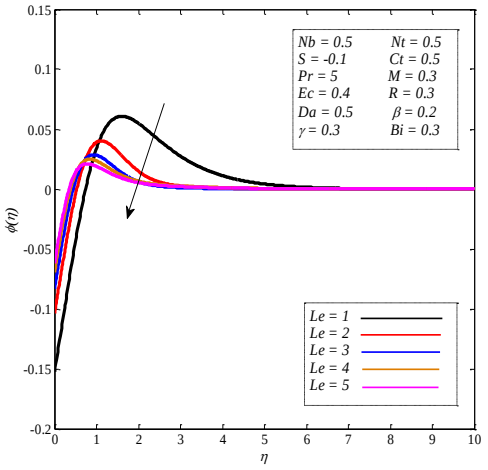

Fig. 12. Effect of the Lewis number Le on the concentration of nanoparticles profile.

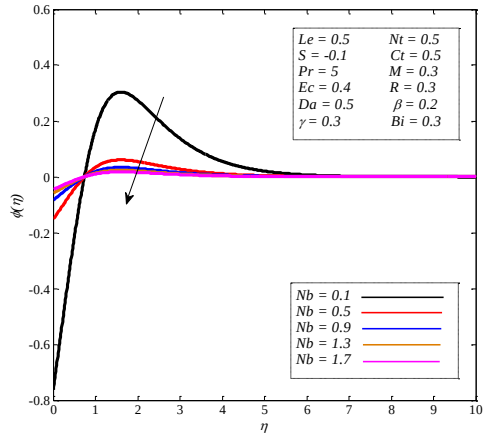

Fig. 13. Effect of the Brownian motion parameter Nb on the concentration of nanoparticles profile.

transfer compared to the total transition and consequently the concentration profiles are diminished. In addition, the Brownian random motion $0.1 \leq Nb \leq 1.7$ means movement of the nanoparticles in the fluid in all directions and this directly gives decrease to concentration of these particles. Therefore, as it can be seen from Fig.13, the growth in the Brownian motion parameter Nb causes a reduction in the concentration of nanoparticles profile.

Moreover, in Figs.14 and 15, effects of the thermophoresis parameter $0.1 \leq Nt \leq 1.7$ on profiles of temperature and concentration of nanoparticles are displayed. Positive effects of Nt are noted and these are due to acquisition of the liquid particles on a temperature which increases the thermal energy and consequently increases the thickness of the boundary layer and increases the concentration of nanoparticles in the fluid as well.

Figures 16 and 17 explain effects of the heat source/sink parameter $-0.3 \leq S \leq 0.01$ on the profiles of temperature and the concentration of nanoparticles. It is clear that a growth in the distributions of both temperature and concentration of nanoparticles is markedly significant when the convective mode is changed from a heat sink $-0.3 \leq S \leq 0$ to a heat source $0 \leq S \leq 0.01$. Physically,

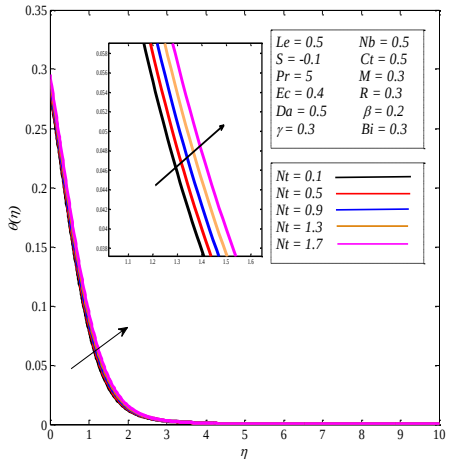

Fig. 14. Effect of the thermophoresis parameter Nt on the temperature profile.

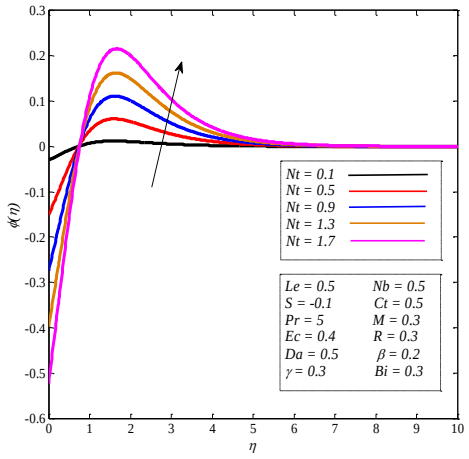

Fig. 15. Effect of the thermophoresis parameter Nt on the concentration of nanoparticles profile.

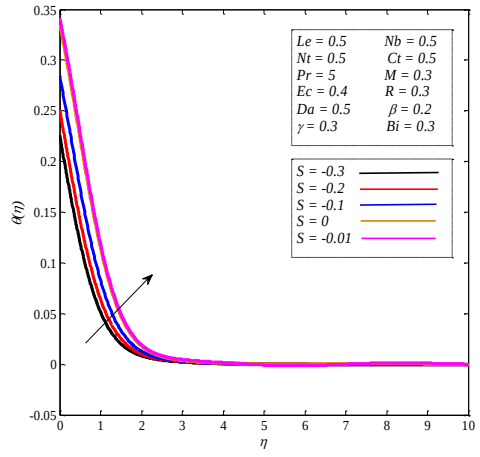

Fig. 16. Effect of the heat source/sink parameter S on the temperature profile.

for heat source it can be seen that the boundary layer generates an additional energy which causes an enhancement in the temperature. However, in the case of heat sink, the convective mode absorbs the heat which decreases pro

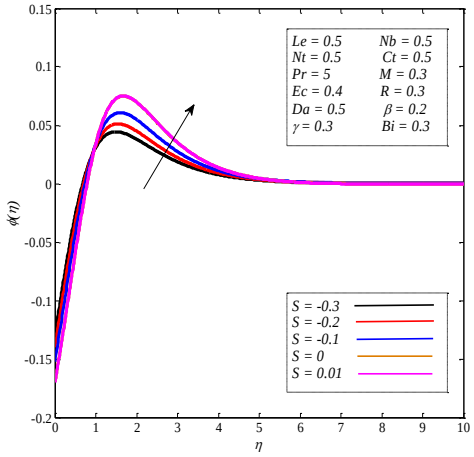

Fig. 17. Effect of the heat source/sink parameter S on the concentration of nanoparticles profile.

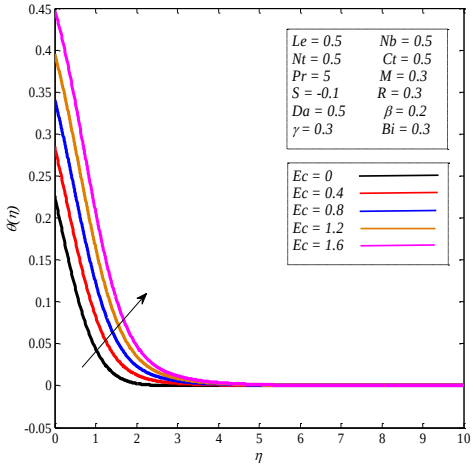

Fig. 18. Temperature profile for variations of the Eckert number Ec.

files of the temperature. For all cases, the increase in values of the heat source/sink parameter supports the concentration of nanoparticles.

Figures 18 and 19 show features of the temperature and concentration of nanoparticles for the values of the Eckert number $0 \leq Ec \leq 1.6$. It is clear that the increase in the distributions of both the temperature and the concentration follows an increase in the values of Ec. Physically, the Eckert number controls movement of the random nanoparticles within the boundary layer, which acts as a marker to increase the fluid temperature due to its high viscosity.

In the same context, Figs. 20 and 21 explain impacts of the Darcy number $0 \leq Da \leq 1.3$ on the profiles of the velocity and the concentration of nanoparticles. It is found that an increment in Da leads to a raise in the distribution of the concentration of nanoparticles while the velocity is reduced. Physically, the increase in Da means lower values of the permeability of the fluid in the porous medium which reduces its movement and the collision of nanoparticles in the porous medium gaining high thermal energy and increases the concentration of nanoparticles.

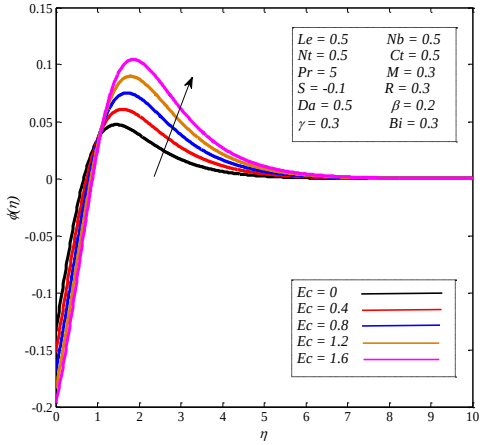

Fig. 19. Concentration profile for variations of the Eckert number Ec.

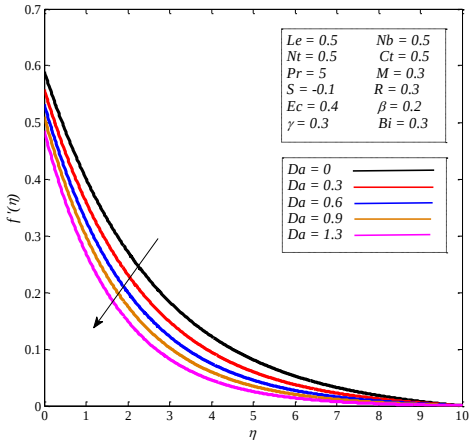

Fig. 20. Velocity profile for variations of the Darcy number Da.

Also, Figs. 22 and 23 present influences of the parameter $0.1 \leq \gamma \leq 1$ on the velocity, temperature and concentration of nanoparticles profiles. It is clear that effects of the parameter γ on the velocity of Casson nanofluid are negative but on the temperature and the concentration of nanoparticles distributions are positive. Additionally, Fig. 24 elucidates effects of the Biot number $0.1 \leq Bi \leq 0.5$ on the temperature and the concentration of nanoparticles distributions. It is clear that an increase in values of Bi means an enhancement in both of the temperature and the concentration of nanoparticles distributions.

On the other side, Fig. 25 observes the gradually decrease in the skin friction profiles when the values of M and Da are increasing. Figure 26 shows that the boost in the heat source/sink parameter S, non-linear thermal radiation parameter R causes a decreasing in the local Nusselt numbers. Finally, Fig. 27 shows effect of the different values of the Prandtl number Pr and the non-linear thermal radiation parameter R on the local Nusselt number. It was found that the enhancement in the values of both Pr and R lead to increase in the local Nusselt number.

D. Numerical solutions

The fourth order Runge–Kutta method is applied to solve the similar Eqs. (9-11) with the boundary conditions (12) and (13). This method starts with reducing order of the differential equations by introducing new variables as follows:

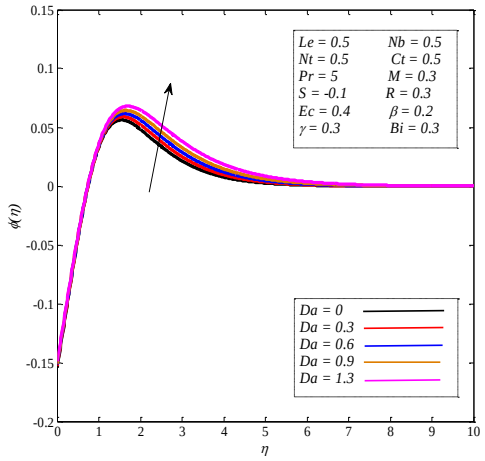

Fig. 21. Concentration of nanoparticles profile for variations of the Darcy number Da.

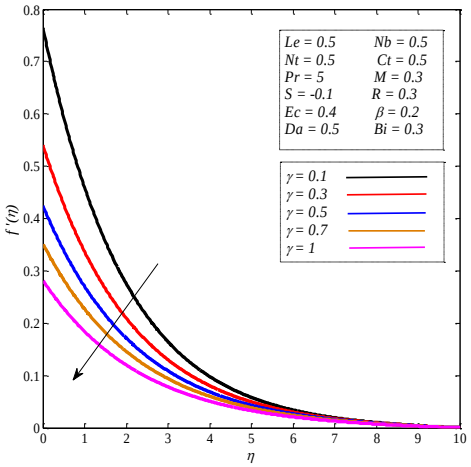

Fig. 22. Velocity profile for variations of γ parameter.

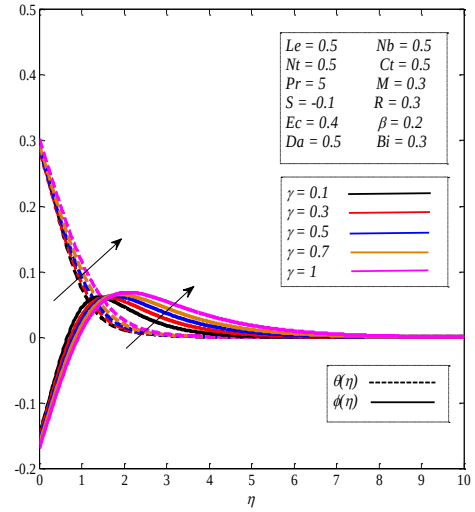

Fig. 23. Temperature and concentration of nanoparticles profiles for variations of γ parameter

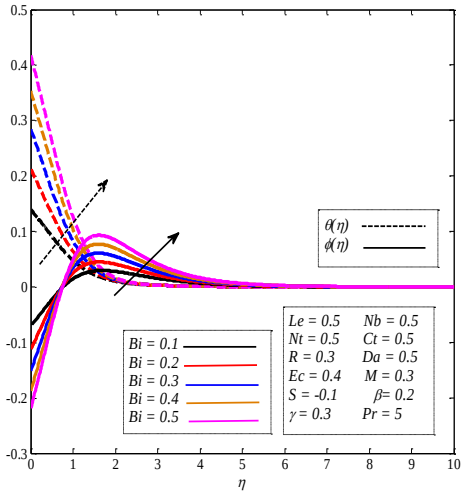

Fig. 24. Temperature and concentration of nanoparticles profiles for variations of Biot number parameter Bi.

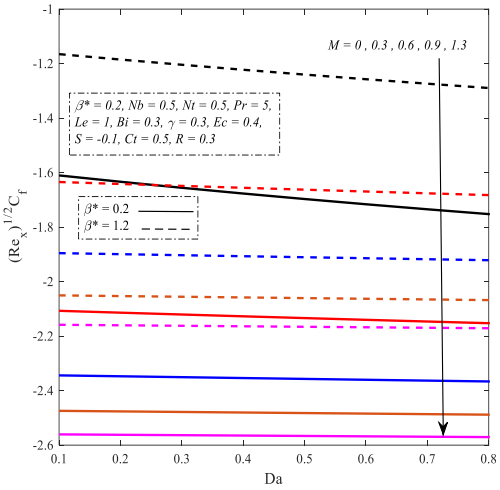

Fig. 25. Effects of magnetic field M and Darcy number Da on the skin friction coefficient.

$$F(1) = F(2),$$
$$F(2) = F(3),$$
$$F(3) = -\left(\frac{\beta}{1+\beta}\right)(-Y(2)^2 + Y(1)Y(3) - (M + Da)Y(2)),$$
$$F(4) = F(5),$$
$$F(5) = -Pr\Big(SY(4) + NbY(5)Y(7) + NtY(5)^2 + 3R\big(Ct + Y(4)\big)^2 Y(5)^2 + EcMY(2)^2 + Y(1)Y(5)\Big)/(1 + PrR(Ct + Y(4))^3)$$
$$F(6) = F(7),$$
$$F(7) = -LeY(1)Y(7) - (Nt/Nb)\,F(5),$$

with the knowledge that

$$f(\eta) = Y(1),$$
$$f'(\eta) = Y(2) = \frac{df(\eta)}{d\eta} = \frac{dY(1)}{d\eta} = F(1),$$
$$f''(\eta) = Y(3) = \frac{d^2 f(\eta)}{d\eta^2} = \frac{dY(2)}{d\eta} = F(2),$$
$$f'''(\eta) = \frac{d^3 f(\eta)}{d\eta^3} = \frac{dY(3)}{d\eta} = F(3),$$
$$\theta(\eta) = Y(4),$$
$$\theta'(\eta) = Y(5) = \frac{d\theta(\eta)}{d\eta} = \frac{dY(4)}{d\eta} = F(4),$$

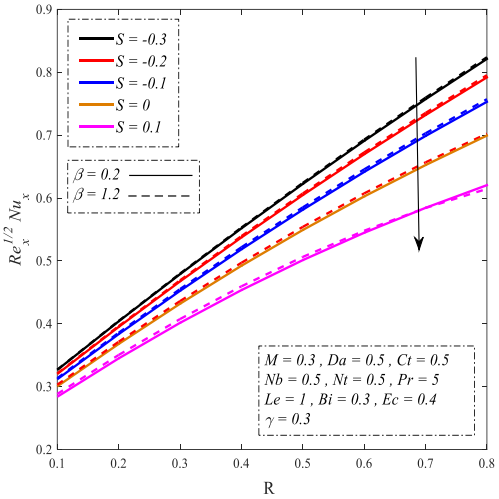

Fig. 26. Effects of heat source/sink parameter S and non-linear thermal radiation R on the local Nusselt number.

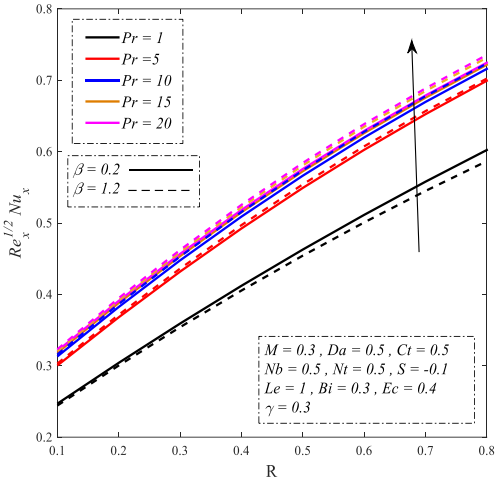

Fig. 27. Effects of Prandtl number Pr and non-linear thermal radiation R on the local Nusselt number.

$$\theta''(\eta) = \frac{d^2\theta(\eta)}{d\eta^2} = \frac{dY(5)}{d\eta} = F(5),$$
$$\phi(\eta) = Y(6),$$
$$\phi'(\eta) = Y(7) = \frac{d\phi(\eta)}{d\eta} = \frac{dY(6)}{d\eta} = F(6),$$
$$\phi''(\eta) = \frac{d^2\phi(\eta)}{d\eta^2} = \frac{dY(7)}{d\eta} = F(7),$$

then the shooting technique is used through the computations. Number of the grid points are equal 500 and η_{max} is equal 10 and hence the step size is 2×10^{-2}. In addition, the convergence criteria are chosen to be equal 10^{-5}. Validations tests are conducted and presented in Tables 1 and 2. It is noted that excellent agreements were found between the presented results (in special cases) and those obtained by Kamran *et al.* (2017).

III. CONCLUSIONS

Magnetohydrodynamic flow of Casson nanofluid over a stretching surface in the presence of heat generation/absorption, non-linear thermal radiation and slip boundary conditions effects has been investigated. Self-similar solutions are obtained for the governing equations and the

Table 1. Comparison between the values of local Nusselt number $-\theta'(0)$ for Kamran *et al.* (2017) and our present study for the values of Nb and M when $\beta = Le = 1, Nt = 0.1, Bi = 0.2, \gamma = 0.3, Ec = 0.5, Pr = 0.71$ in absence of Da, S, R and Ct.

$Nb = 0.1$	Kamran *et al.* (2017)	Present study	$M = 0.5$	Kamran *et al.* (2017)	Present study
M	$-\theta'(0)$	$-\theta'(0)$	Nb	$-\theta'(0)$	$-\theta'(0)$
0.2	0.1262	0.1262	0.1	0.1142	0.1142
0.5	0.1141	0.1142	0.3	0.1097	0. 1098
0.7	0.1071	0.1073	0.5	0.1052	0. 1053
1	0.0979	0.0982	0.9	0.0956	0. 0957

Table 2. Comparison between the values of local Nusselt number $-\theta'(0)$ for Kamran *et al.* (2017) and our present study for the values of Nt and Pr when $\beta = Le = 1$, $Nb = 0.1$, $Bi = 0.2$, $\gamma = 0.3$, $Ec = 0.5$, $M = 0.5$ in absence of Da, S, R and Ct.

$Pr = 0.71$	Kamran *et al.* (2017)	Present study	$Nt = 0.1$	Kamran *et al.* (2017)	Present study
Nt	$-\theta'(0)$	$-\theta'(0)$	Pr	$-\theta'(0)$	$-\theta'(0)$
0.1	0.1141	0.1142	0.71	0.1141	0.1142
0.3	0.1130	0.1131	2	0.1307	0.1306
0.5	0.1119	0.1120	5	0.1344	0.1344
0.9	0.1096	0.1096	8	0.1328	0.1328

resulting system of equations is solved using the shooting technique. Comparisons between the Newtonian nanofluid and non-Newtonian Casson nanofluid cases are performed and wide ranges of the governing parameters are assumed. The important findings in this study can be summarized as follows:

- The velocity decreases by the increase in values of the magnetic field parameter M, Darcy number Da, Casson fluid parameter β and the γ parameter.
- The temperature in the boundary layer is enhanced by an increment in the γ parameter, Eckert number Ec, magnetic field parameter M, Darcy number Da, thermophoresis parameter Nt, Biot number Bi, non-linear thermal radiation parameter R and the Ct parameter.
- The concentration of nanoparticles is enhanced as the values of the magnetic field parameter M, Darcy number Da, Casson fluid parameter β, γ parameter, thermophoresis parameter Nt, Eckert number Ec, Biot number Bi and the heat source/sink parameter S are increased.
- Enhancements in the Nusselt number values are obtained as a result of the increase in values of the thermal radiation parameter R, Prandtl number Pr and the Casson fluid parameter β while the reverse effect is given in case of the heat source/sink parameter S.
- The increasing in the magnetic field parameter M and the Darcy number Da lead to decreasing in the skin friction coefficient.

ACKNOWLEDGMENT

The authors extend their appreciation to the Deanship of Scientific Research at King Khalid University for funding this work through research groups program under Grant Number (R.G.P2/27/42)

NOMENCLATURE

a Stretching rate.
Bi Biot number.
C Concentration of nanoparticles.
C_f Skin friction coefficient.
C_w Nanoparticles fraction at wall.
C_∞ Stream concentration.
C_t Ratio temperature parameter.
Da Darcy number.
D_B Brownian diffusion coefficient.
D_T Thermophoresis diffusion coefficient.
Ec Eckert number.
e_{ij} Deformation rate.
$f'(\eta)$ Velocity function.
h Coefficient of convective heat transfer.
K Permeability.
k^* Mean absorption coefficient.
k Thermal conductivity.
Le Lewis number.
M Magnetic field parameter.
Nb Brownian motion parameter.
Nt Thermophoresis parameter.
Nu_x Local Nusselt number.
Pr Prandtl number.
Q Dimensional heat generation/absorption.
q_r Nonlinear radiative heat flux.
q_w Heat flux.
q_m Mass flux.
R Non-linear thermal radiation parameter.
Re_x Local Reynolds number.
S Heat source/sink parameter.
Sh_x Local Sherwood number.
T Temperature.
T_w Temperature at wall.
T_∞ Stream temperature.
U_w Stretching sheet velocity.
u, v Velocity components.
x, y Space coordinates.

Greek Symbols

α Thermal diffusivity.
β Casson fluid parameter.
γ Nondimensional slip velocity parameter.
η Similarity variable.
$\theta(\eta)$ Dimensionless temperature function.
ν Kinematic viscosity
ρ Density of the fluid
σ^* Stefan-Boltzmann constant.
τ Ratio of the effective heat capacity of nanoparticle material to the effective heat capacity of the base fluid.
τ_w Shear stress along the stretching sheet.
$\phi(\eta)$ Dimensionless concentration of nanoparticles function.
μ Dynamic viscosity.
μ_p Plastic dynamic viscosity
π Product of the component of deformation rate with itself.
π_c Critical Product of the component of deformation rate with itself.

REFERENCES

Chamkha, A.J. and Aly, A.M. (2010) MHD free convection flow of a nanofluid past a vertical plate in the presence of heat generation or absorption effects. *Chemical Engineering Communications*. **198**, 425-441.

Chamkha, A., Aly, A.M. and Al-Mudhaf, H.F. (2011) Laminar MHD mixed convection flow of a nanofluid along a stretching permeable surface in the presence of heat generation or absorption effects. *International Journal of Microscale and Nanoscale Thermal*. **2**, 51-70.

Gaffar, S.A., Prasad, V.R., Reddy, E.K. and Bég, O. (2015) Thermal radiation and heat generation/absorption effects on viscoelastic double-diffusive convection from an isothermal sphere in porous media. *Ain Shams Engineering Journal*, **6**, 1009-1030.

Hayat, T., Sajjad, R., Abbas, Z., Sajid, M. and Hendi, A.A. (2011) Investigated radiation effects on MHD flow of Maxwell fluid in a channel with porous medium. *International Journal of Heat and Mass Transfer*, **54**, 854–862.

Hayat, T., Shehzad, S.A., Alsaedi, A. and Alhothuali, M.S. (2013) Three dimensional of Oldroyd-B fluid over surface with convective boundary conditions. *Appl. Math. Mech*. **34**, 489–500.

Hayat, T., Qayyum, S., Shehzad, S. A. and Alsaedi, A. (2018) Cattaneo-Christov double-diffusion theory for three-dimensional flow of viscoelastic nanofluid with the effect of heat generation/absorption. *Results in Physics*. **8**, 489–495.

Ibrahim, S.M., Lorenzini, G., Kumar, P.V. and Raju, C.S.K. (2017) Influence of chemical reaction and heat source on dissipative MHD mixed convection flow of a Casson nanofluid over a nonlinear permeable stretching sheet. International Journal of Heat and Mass Transfer. **111**, 346-355.

Kamran, A., Hussain, S., Sagheer, M. and Akmal, N. (2017) A numerical study of magnetohydrody-namics flow in Casson nanofluid combined with Joule heating and slip boundary conditions. *Results in Physics*, **7**, 3037–3048.

Kataria, H.R. and Mittal, A.S. (2017) Velocity, mass and temperature analysis of gravity-driven convection nanofluid flow past an oscillating vertical plate in the presence of magnetic field in a porous medium. *Applied Thermal Engineering*. **110**. 864-874.

Kataria, H. R. and Patel, H. R. (2018) Heat and mass transfer in magnetohydrodynamic (MHD) Casson fluid flow past over an oscillating vertical plate embedded in porous medium with ramped wall temperature. *Propulsion and Power Research*, **7**, 257-267.

Kataria, H.R. and Patel, H.R. (2019a) Effects of chemical reaction and heat generation/absorption on magneto-hydrodynamic (MHD) Casson fluid flow over an exponentially accelerated vertical plate embedded in porous medium with ramped wall temperature and ramped surface concentration. *Propulsion and Power Research.* **8**, 35-46.

Kataria, H.R., and Patel, H.R. (2019b) Effects of chemical reaction and heat generation/absorption on magneto-hydrodynamic (MHD) Casson fluid flow over an exponentially accelerated vertical plate embedded in porous medium with ramped wall temperature and ramped surface concentration. *Propulsion and Power Research*. **8**, 35-46.

Kumar, K.G., Rahimi-Gorji, M., Reddy, M.G., Chamkha, A.J. and Alarifi, I.M. (2020) Enhancement of heat transfer in a convergent/divergent channel by using carbon nanotubes in the presence of a Darcy–Forchheimer medium. *Microsystem Technologies*. **26**, 323–332.

Kumaran, G. and Sandeep, N. (2017) Thermophoresis and Brownian moment effects on parabolic flow of MHD Casson and Williamson fluids with cross diffusion. *Journal of Molecular Liquids*. **233**, 262-269.

Mehryan, S.A.M., Izadi, M., Chamkha, A.J. and Sheremet, M.A. (2018) Natural convection and entropy generation of a ferrofluid in a square enclosure under the effect of a horizontal periodic magnetic field. Journal of Molecular Liquids. **263**, 510-525.

Mehryan, S.A.M., Sheremet, M.A., Soltani, M. and Izadi, M. (2019) Natural convection of magnetic hybrid nanofluid inside a double-porous medium using two-equation energy model. *Journal of Molecular Liquids*. **277**, 959-970.

Nawaz, M., Naz, R. and Awais, M. (2018) Magneto-hydrodynamic axisymmetric flow of Casson fluid with variable thermal conductivity and free stream. *Alexandria Engineering Journal*. **57**, 2043-2050.

Pal, D., Roy, N. and Vajravelu, K. (2016) Effects of thermal radiation and Ohmic dissipation on MHD Casson nanofluid flow over a vertical non-linear stretching surface using scaling group transformation. *International Journal of Mechanical Sciences*. **114**, 257-267.

Palaniammal, S. and Saritha, K. (2018) MHD viscous Casson fluid flow in the presence of a temperature gradient dependent heat sink with prescribed heat and mass flux. *Frontiers in Heat and Mass Transfer (FHMT)*. **10**, 1.

Pop, I., M., Sheremet (2016) Free convection in a square cavity filled with a Casson fluid under the effects of thermal radiation and viscous dissipation. *International Journal of Numerical Methods for Heat & Fluid Flow*. **27**, 2318-2332.

Prasad, K.V., Vajravelu, K., Vaidya, H., Basha, N.Z. and Umesh, V. (2018) Thermal and species concentration of MHD Casson fluid at a vertical sheet in the presence variable fluid properties. *Ain Shams Engineering Journal*. **9**, 1763-1779.

Ramzan, M., Inam, S. and Shehzad, S.A. (2016) Three-dimensional boundary layer flow of a viscoelastic nanofluid with Soret and Dufour effects. *Alexandria Engineering Journal*. **55**, 311–319.

Reddy, P. B. A. (2016) Magnetohydrodynamic flow of a Casson fluid over an exponentially inclined permeable stretching surface with thermal radiation and

chemical reaction. *Ain Shams Engineering Journal*. **7**. 593-602.

Reddy, G.J., Raju, R.S. and Rao, J.A. (2018a) Influence of viscous dissipation on unsteady MHD natural convective flow of Casson fluid over an oscillating vertical plate via FEM. *Ain Shams Engineering Journal*. **9**, 1907-1915.

Reddy, G.J., Kethireddy, B., Umavathi, J.C., and Sheremet, M.A. (2018b) Heat flow visualization for unsteady Casson fluid past a vertical slender hollow cylinder. *Thermal Science and Engineering Progress*. **5**, 172-181.

Rehman, K.U., Malik, M.Y., Zahri, M. and Tahir, M. (2018) Numerical analysis of MHD Casson Navier's slip nanofluid flow yield by rigid rotating disk. *Results in Physics*. **8**, 744-751.

Saqib, M., Khan, I. and Shafie, S. (2018) Application of Atangana–Baleanu fractional derivative to MHD channel flow of CMC-based-CNT's nanofluid through a porous medium. *Chaos, Solitons & Fractals*. **116**, 79-85.

Seth, G.S., Kumar, R. and Bhattacharyya, A. (2018) Entropy generation of dissipative flow of carbon nanotubes in rotating frame with Darcy-Forchheimer porous medium: A numerical study. *Journal of Molecular Liquids*. **268**, 637-646.

Shit, G.C., Haldar, R. and Mandal, S. (2017) Entropy generation on MHD flow and convective heat transfer in a porous medium of exponentially stretching surface saturated by nanofluids. *Advanced Powder Technology*. **28**, 1519-1530.

Souayeh, B., Reddy, M.G., Sreenivasulu, P., Poornima, T. and Alarifi, I.M. (2019) Comparative analysis on non-linear radiative heat transfer on MHD Casson nanofluid past a thin needle. *Journal of Molecular Liquids*. **284**, 163-174.

Sulochana, C., Samrat, S.P. and Sandeep, N. (2018) Magnetohydrodynamic radiative liquid thin film flow of kerosene based nanofluid with the aligned magnetic field. *Alexandria Engineering Journal*. **57**, 3009-3017.

Tamoor, M., Waqas, M., Khan, M.I., Asaedi, A. and Hayat, T. (2017) Magnetohydrodynamic flow of Casson fluid over a stretching cylinder. *Results in Physics*. **7**, 498-502.

Ullah, I., Shafie, S., Makinde, O.D. and Khan, I. (2017) Comment on the paper Unsteady MHD Falkner-Skan flow of Casson nanofluid with generative/destructive chemical reaction. *Chemical Engineering Science*. **172**, 694–706.

Received: January 14, 2020
Sent to Subject Editor: July 7, 2020
Accepted: June 18, 2021
Recommended by Subject Editor Fabio Giannetti